Air–Sea Heat Flux Measurements from Nearly Neutrally Buoyant Floats

ERIC A. D'ASARO

Applied Physics Laboratory and School of Oceanography, University of Washington, Seattle, Washington

(Manuscript received 18 October 2002, in final form 27 November 2003)

ABSTRACT

The ability of neutrally buoyant, high-drag floats to measure the air–sea heat flux from within the turbulent oceanic boundary layer is investigated using float data from four different winter and fall float deployments. Two flux estimates can be made: Q_{0A} measures the vertical advection of heat, and Q_{0D} integrates the Lagrangian heating rate. Because the floats are only imperfectly Lagrangian, a key issue is diagnosing the ability of a given set of float data to make accurate flux measurements. A variety of diagnostics are explored and evaluated. Here Q_{0A} and Q_{0D} are compared to heat flux measurements computed using bulk formulas and shipboard measurements for one 2-week cruise. Quality controlled float-based fluxes agree with bulk fluxes to within 10 W m^{-2} for both positive and negative values. The differences are well within the expected statistical errors in the float measurements and the bias errors of the bulk measurements.

1. Introduction

Direct measurements of air–sea fluxes have been made almost entirely from the air side of the interface. For example, covariance heat flux measurements require the measurement of $\langle wT' \rangle$, where w is the vertical velocity, T is a temperature, and the angle brackets ($\langle\ \rangle$) denote a time or space average chosen so that $T' = T - \langle T \rangle$, $\langle T' \rangle = 0$, and $\langle w \rangle = 0$. Difficulties typically arise in defining the vertical direction, defining appropriate time scales for $\langle\ \rangle$, and in measuring T and w with sufficient accuracy and rapidity, particularly in the presence of large surface waves. Nevertheless, recent advances have allowed heat and humidity fluxes to be computed accurately near the air–sea interface under a wide range of conditions (e.g., Graber et al. 2000; Edson et al. 1998).

Similar measurements on the ocean side of the interface can be more difficult. In particular, the typical turbulent velocity fluctuations in the oceanic boundary layer are centimeters per second, much smaller than the meters per second velocities of the surface waves. This makes the measurement of w difficult. Furthermore, the accelerations of surface waves are comparable to that of gravity (hence the phenomenon of seasickness) making the definition of ''vertical'' nontrivial. These problems have prevented the direct measurement of air–sea fluxes from the water side of the interface in the open ocean.

Corresponding author address: Dr. Eric A. D'Asaro, Applied Physics Laboratory, University of Washington, 1013 NE 40th St., Seattle, WA 98105.
E-mail: dasaro@apl.washington.edu

Here, the measurement of heat fluxes from neutrally buoyant floats in the upper ocean boundary layer is discussed. These floats measure pressure and temperature and are engineered to accurately follow the three-dimensional trajectories of water parcels in a turbulent fluid (see D'Asaro 2003a for details). The pressure measured by the float is used to determine its depth. Vertical velocity is computed from the rate of change of pressure. Because pressure fluctuations are zero along particle paths for linear surface waves and surface waves are nearly linear, the surface wave pressure fluctuations measured by Lagrangian floats are greatly attenuated from their Eulerian values (D'Asaro et al. 1996; D'Asaro 2001). The pressure measured by the float therefore closely measures its depth below mean sea level. Furthermore, the periods of surface waves, typically 10 s, are much faster than the ''large eddy'' periods in the mixed layer, typically 1 h for a 20-m mixed layer, so that the remaining wave-induced fluctuations can be averaged effectively. Because the average pressure surfaces in the ocean are parallel to the mean surface, the time derivative of pressure gives the motion of the float perpendicular to the mean surface and is thus the correct ''vertical'' velocity to use in flux measurements. Lagrangian floats can thus potentially overcome the major problems facing flux measurements in the upper ocean.

Not surprisingly, float measurements have some inherent difficulties. Sensor accuracy is not a major issue; measurements of pressure to 0.01 db and temperature to 1 mK are relatively easy to make and sufficient. The finite size of the float acts as a low-pass filter, thus limiting the frequency response of the float (Lien et al.

1998), but not in the frequency range that is important for flux estimates. Most importantly, however, real floats almost always have some residual buoyancy, which induces motion relative to the surrounding water. The computation of Eulerian statistics, such as heat flux profiles, requires that the float trajectories randomly sample each level in an unbiased manner. For turbulent flows, this is a reasonable assumption if the floats are neutrally buoyant. However, if floats are not neutrally buoyant, their buoyancy causes the sampling to be biased (D'Asaro et al. 2002; Harcourt et al. 2002; Lherminier et al. 2001). Buoyant floats, for example, tend to oversample trajectories with strong near-surface downward velocities and temperature anomalies, and thus measure larger heat fluxes.

The goals here are to compare fluxes and kinetic energies measured by floats with those measured by bulk methods, to assess the errors in float measurements due to their buoyancy, and to develop methods for quantifying these errors. Section 2 describes the floats and their data. Section 3 describes the methods used to compute vertical kinetic energy and surface heat flux from the floats as well as several diagnostics to assess the extent to which floats are Lagrangian. Section 4 compares float-derived surface heat fluxes with those computed from shipboard measurements. Section 5 summarizes these results and discusses the prospects for making routine long-term heat flux measurements from Lagrangian floats.

2. Data

a. Lagrangian floats

Data from three float deployments using three different varieties of Lagrangian floats are used here. The Lagrangian floats were constructed at the Applied Physics Laboratory, University of Washington. They are an approximately meter-long cylinder, 12–20 cm in diameter with a displacement of 15–50 L. A horizontal circular disk of approximately 1 m^2 is attached to add additional vertical drag. All floats measure pressure and temperature; some measure additional quantities. Details of float construction and behavior are provided in D'Asaro (2003a) and D'Asaro et al. (1996).

b. 1995 MLF deployments—North Pacific

Lagrangian float deployments were made on 11–31 January 1995 in the eastern North Pacific (approximately 48.2°N, 127.8°W) during a series of moderate winter storms. Meteorological measurements made from the R/V *Wecoma* were used to compute air–sea fluxes using the bulk formulas described in Dickey et al. (1994). D'Asaro (2001) describes these measurements in more detail. Mixed layer depths were 40–70 m, typical float vertical velocities were 0.01–0.02 m s^{-1}, and typical turnover times, as measured by the floats' motion, were a few thousand seconds. A strong correlation between vertical kinetic energy and wind stress was found, despite strong variations in the surface wave field.

Three mixed layer Lagrangian floats (MLFs; D'Asaro et al. 1996) were used. Each was deployed from the ship, gathered data for about 24 h, was recovered, and then redeployed. Each deployment used a different drop weight and the batteries were changed periodically. The volume and weight of each float were carefully adjusted on each deployment to compensate for these changes so that the error due to them was at most a few grams. The total variation of mixed layer density was only about 0.03 kg m^{-3}, corresponding to only about a 0.6-g float buoyancy change. It was difficult, however, to precisely match the density of the float to that of the mixed layer. Instead, each float's buoyancy was varied during the first few deployments until the distribution of float depths was only slightly surface intensified. As will be discussed in detail below, this indicated that the float was slightly buoyant and would thus not sink into the thermocline. The float buoyancy was then maintained at approximately this value throughout the cruise. The best guess is that the floats were typically a few grams light on average with a random variation of a few grams between deployments.

c. 1997–98 DLF deployments—Labrador Sea

Lagrangian float deployments were made from 12 February to 14 March 1997 and 26 January to 24 March 1998 in the Labrador Sea as part of the Labrador Sea Deep Convection Experiment (Lab Sea Group 1998). Data from 15 deep Lagrangian floats (DLFs; Steffen and D'Asaro 2002) were used. Air–sea fluxes were computed from the National Centers for Environmental Prediction (NCEP) model runs; there was considerable uncertainty in their accuracy (Renfrew et al. 2002). Mixed layer depths were 500–1000 m, typical float vertical velocities were 0.01–0.02 m s^{-1}, and typical overturning times were 1–2 days. The vertical kinetic energy could be predicted well from the surface heat flux based on theories of convective turbulence.

It was not possible to assess the buoyancy of the 1997 floats. In 1998, however, the floats spent the first month of their mission just below the mixed layer and were eventually entrained into it as it deepened. The floats' densities within the mixed layer can be computed from their known physical properties (D'Asaro 2003a), the manner in which they changed their own density, the ocean stratification, and the time history of their density before entrainment. The effect of ocean stratification is small. The floats steadily lost buoyancy for a total loss of about 1 g of buoyancy during the 60 days of measurement. D'Asaro (2003a) suggests that this is due to chemical reactions between the float surface and seawater. The most important effect, however, was the change of float buoyancy with pressure. The combi-

nation of hull compressibility and programmed changes in float volume made the floats slightly more compressible than seawater. Assuming the floats to be neutral at the bottom of the convective layer, their buoyancy decreased at a rate of 0.28 g (100 db)$^{-1}$. In addition, up to 5 cc of air trapped in float crevices and O-rings (D'Asaro 2003a) affected the buoyancy. The average float buoyancy in the 600-db deep convective layer is estimated at 0.8 g (heavy) assuming no air and about 0.5 g (heavy) assuming 5 cc of air.

For both the 1997 and 1998 data, only periods when the floats were actively convecting were used in the analysis. In the 1997 data the initial autoballasting period only was discarded. In the 1998 data many of the floats convected only intermittently. These convective periods were hand selected. A few of the resulting trajectories were too short to be useful and have been ignored here. Some of the longer ones, in both 1997 and 1998, have been artificially split into two shorter records. The result is 18 records that are 5–14.5 days long.

d. 2000 MLFII deployments—North Pacific

Two second-generation mixed layer floats (MLFIIs; numbers 6 and 7) were deployed in the North Pacific from days 271 to 311 (28 September–7 November 2000). During this time the mixed layer evolved from approximately 30- to approximately 55-m depth. This model of float (D'Asaro 2003a) was significantly heavier (50 kg) than the DLF (15 kg) or MLF (20 kg), and carried two CTDs separated by 1.4 m and a Doppler sonar, which measured the water velocity relative to the float at approximately the location of the top CTD with an accuracy of about 1 mm s^{-1}. Ballasting was accomplished by allowing the float to settle to the level of its own density near 170 db. The CTD and the physical properties of the float were then used to adjust the float's density to that of the mixed layer. The quality of the ballasting varied due to errors in the method, mechanical errors in setting the float volume, drift of the CTD calibration, and uncertainty in the parameters used. The variations are estimated at a few grams of buoyancy.

Each day of the mission was divided into four approximately 4-h-long Lagrangian drifts, separated by three profiles to approximately 130 db and one profile to approximately 170 db. Only data from the Lagrangian drifts are used here. For each, a mixed layer depth was defined from the surrounding profiles based on the first deviation of σ_θ by more than 0.05 kg m^{-3} from its average value between 15 and 20 db. Only drift segments for which the float spent more than 80% of the time above the mixed layer depth were used. Statistics were computed on groups of 20 consecutive valid drift segments, that is, approximately 5 days of float data from each float. This resulted in 13 analyzed segments out of a possible 16 from 80 float days of data.

3. Computations

a. Interpolation and averaging

Lagrangian data taken uniformly in time are necessarily spaced irregularly in position and must be interpolated to place data at a given depth. Near the surface, some float statistics, notably Φ_D and σ_{wA} (see below), vary rapidly with depth and are therefore sensitive to the details of data interpolation. Accordingly, all depth-dependent float statistics were computed by linearly interpolating between the measured data points and evaluating the appropriate statistic exactly from this interpolated function. D'Asaro (2003b) describes this in more detail. Depth-averaged statistics were computed using float data shallower than a mixed layer depth H taken as 45 m for the 1995 MLF data, 600 m for the 1997–98 DLF data, and a depth-variable function for the MLFII 2000 data.

Confidence limits for all quantities were computed using a bootstrap method (Efron and Gong 1983). For depth-binned quantities, each pass of a float through a given depth bin was considered independent. Bootstrap confidence limits for the mean of the quantity were computed from the ensemble of values. For quantities that were computed from a profile, for example a line fit or integral, each realization of the profile was created by randomly selecting a measured value from each depth bin. Typically, 300 bootstrap realizations were created.

b. Depth distribution

Figure 1 shows data from a DLF deployed in the Labrador Sea in 1997. Under the influence of strong surface cooling (Fig. 1a), the float repeatedly cycles through a convective layer 600–1000 m deep (Fig. 1b). These plumes carry cooled water down from the surface and thus cool the boundary layer (Fig. 1c). The float spends more time near the surface than at depth as can be seen both from the raw trajectories (Fig. 1a) and the distribution of depths $\mathcal{P}(z)$ (Fig. 1d, gray bars). The nonuniformity of $\mathcal{P}(z)$ is quantified by the pressure skewness:

$$\mathcal{S}_Z = \frac{\langle Z - \langle Z\rangle\rangle^3}{\sigma_Z^3}, \tag{1}$$

where the brackets denote a time average over a trajectory, $\langle X\rangle = \int_{-H}^{0} \mathcal{P}(z)X\,dz$, and $\sigma_Z^2 = (Z - \langle Z\rangle)^2$ is the standard deviation of float depth Z. Probability distributions with larger (smaller) values near the surface have $\mathcal{S}_Z > 0$ ($\mathcal{S}_Z < 0$).

The most obvious interpretation of a nonzero $\mathcal{S}_Z$ is that it represents float buoyancy. Clearly, a highly buoyant float will tend to stay near the surface resulting in a $\mathcal{P}(z)$ that is surface intensified and a positive value of $\mathcal{S}_Z$. This is explored in models ranging from Stommel (1949) to Farmer and Li (1995) and Harcourt et al. (2002). Similarly, a heavy float will tend to produce a negative value of $\mathcal{S}_Z$.

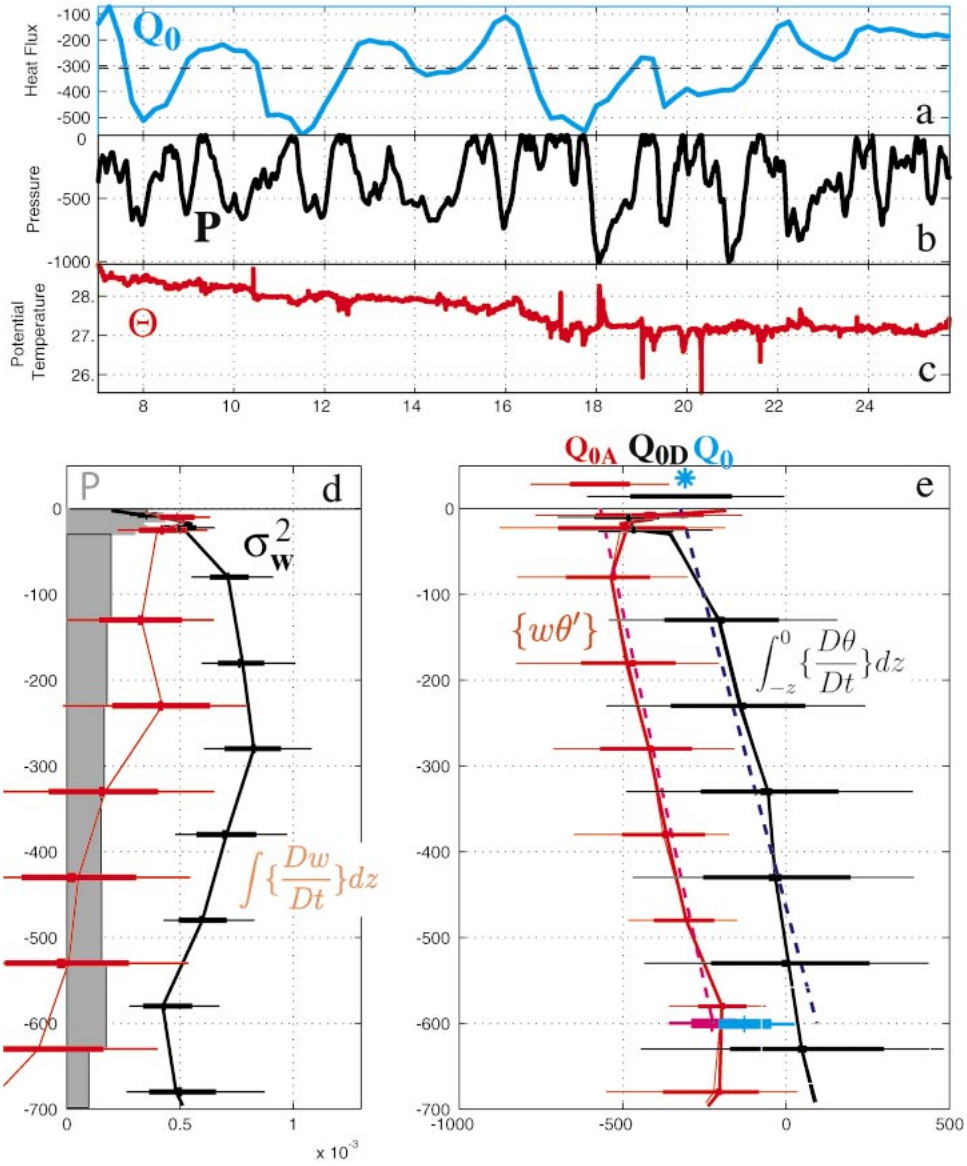

FIG. 1. Analysis of DLF float 8 deployed in the Labrador Sea in Feb 1997. This float was chosen because it is somewhat buoyant and thus illustrates the errors that occur for buoyant floats. (a) Surface heat flux from NCEP analysis. The dashed line gives the average heat flux. (b) Depth–time trajectory. (c) Potential temperature measured on the float. (d) Gray bars, probability distribution of depth $\mathcal{P}(z)$ on an arbitrary scale; black, σ_w^2, the vertical velocity variance; red, σ_{wA}^2, the vertical velocity variance computed from acceleration using (4). (e) Red, the advective heat flux; black, the diffusive heat flux. Lines show fits of these functions. Surface intercept of lines gives surface heat flux estimates Q_{0A} and Q_{0D} plotted above the surface. Blue star gives average bulk heat flux from (a). Error bars in (d) and (e) are 30%, 70%, and 95% from 300 bootstrap realizations. Note that much smaller depth bins (5 m) are used in the upper 30 m than below (100 m).

Other more subtle factors may also contribute to the skewness. First, these floats are operated so as to have the same density as the mixed layer. However, in an entraining mixed layer, such as in the Labrador Sea, water parcels are exchanged between the mixed layer and the underlying stratification. Floats, however, cannot travel into the stratification because they are too light and thus avoid the freshly entrained water. This is more common near the bottom of the mixed layer leading to a deficit of floats as the bottom is approached and a positive $\mathcal{S}_Z$. Similarly, in the MLF 1995 data the floats are confined to a mixing layer that varies in depth from less than 10 m in light winds to about 70 m during strong winds (D'Asaro 2001). Because the mixing layer is always present near the surface but only sometimes present at depth, floats that are uniformly distributed within the mixing layer spend more time near the surface than at depth and have a positive $\mathcal{S}_Z$.

The magnitude of these effects can be investigated using existing data. The Doppler sonar on MLFII 2000 float 6 measured an average along-float (nearly vertical) velocity of 0.5 mm s^{-1}. This drift velocity is much less than the rms vertical float velocity, about 1.5 cm s^{-1}, and implies that the float is well ballasted. The average $\mathcal{S}_z$ is about 0.4, clearly larger than zero. Similarly, Harcourt et al. (2002) simulates the 1997 DLF Labrador Sea data. His centrally ballasted (CBL) floats are nearly neutrally buoyant (0.5 g heavy at the surface and 0.5 g light at 1000 db). Their average $\mathcal{S}_z$ is 0.1–0.2 depending on what mixed layer depth is used, again clearly larger than zero. His buoyantly ballasted (BBL) floats ($\approx$5 g buoyant) have an average $\mathcal{S}_z$ of 0.5. Thus, although the skewness is clearly an indicator of float buoyancy, a float that is neutrally buoyant only in the mixed layer may have a slightly positive skewness due to the variability in mixed layer depth and density.

c. Vertical velocity variance

The equation for vertical acceleration yields two separate estimates of the vertical velocity variance. The accuracy to which these agree provides a measure of how well a given set of float data can sample the boundary layer turbulence.

The vertical acceleration can be written as

$$\frac{Dw}{Dt} = \frac{\partial w}{\partial t} + \frac{1}{2}\frac{\partial w^2}{\partial z} + \nabla_H \cdot (\boldsymbol{u}w), \tag{2}$$

where ∇_H is the horizontal gradient operator. Averaging this in time and horizontally so the second and last terms vanish yields

$$\left\langle \frac{Dw}{Dt} \right\rangle (z) = \frac{\partial}{\partial z}\left\langle \frac{w^2}{2} \right\rangle (z), \tag{3}$$

where the $\langle\ \rangle$ denotes the averaging operation. For Lagrangian data $\langle\ \rangle$ implies selecting all data in a given depth bin and averaging as discussed in section 3a. The profile of $\langle w^2 \rangle(z)$ can be computed either directly, which will be denoted as σ_w^2, or from

$$\langle w^2 \rangle(z) = 2\int_z^0 \left\langle \frac{Dw}{Dt} \right\rangle (z)\, dz, \tag{4}$$

where $w = 0$ at $z = 0$, which will be denoted as σ_{wA}^2.

Figure 1d shows sample profiles of σ_w^2 (black) and σ_{wA}^2 (red). They diverge rapidly in the surface layer and continue to diverge slowly below with σ_{wA}^2 becoming negative below 350 m. The difference between these is quantified by fitting a line to $\Delta\sigma_w^2 = [\sigma_w^2 - \sigma_{wA}^2](z)$ and denoting the fit by $\widehat{\Delta\sigma_w^2}(z)$. A nondimensional measure of the error is

$$E_w = \frac{\widehat{\Delta\sigma_w^2}(H/2)}{H^{-1}\displaystyle\int_{-H}^{0} \sigma_w^2\, dz}. \tag{5}$$

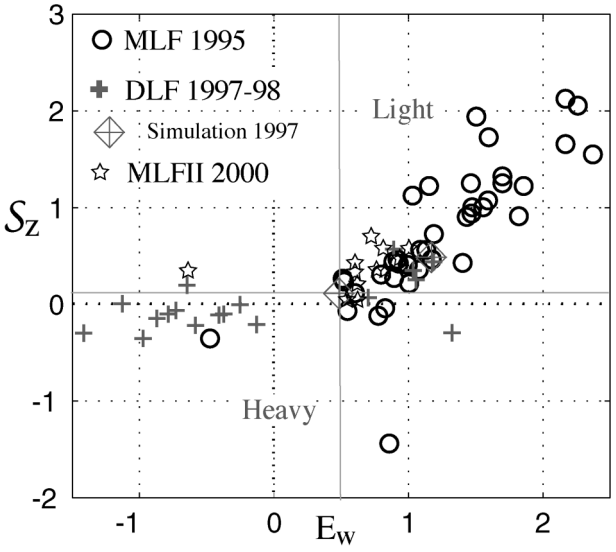

FIG. 2. Comparison of error in vertical momentum equation E_w with skewness of depth probability distribution $\mathcal{S}_z$ for MLF, DLF, MLFII, and simulated (Harcourt et al. 2002) DLF data. Gray lines separate best-guess regions in which floats are heavy from those in which they are light.

Figure 2 compares E_w and $\mathcal{S}_z$. A strong correlation is found: trajectories that spend more (less) time near the surface also have σ_w^2 greater (less) than σ_{wA}^2. This correlation is easy to understand: buoyancy causes the float to turn upward, leaving the water behind, and thus spend more time near the surface. This also makes the float Dw/Dt more positive than that of the water and thus makes σ_{wA}^2 more negative than σ_w^2. The slope of the correlation is much less for heavy floats than for buoyant ones, perhaps because highly buoyant floats can become trapped at the surface, leading to a strong concentration near the surface, while heavier floats just sink deeper into the thermocline and are less strongly concentrated.

Figure 2 also plots the data points for the Harcourt et al. (2002) simulated nearly neutral CBL floats and his 5-g buoyant BBL floats. These have E_w of 0.46 and 1.1, respectively. They fall on curves defined by the ocean data. Note that the neutrally buoyant floats do not have zero E_w. Also, the 1998 DLFs are all heavy. Consistent with this, the BBL point is to the right and above all of these. These results suggest a division of the E_w and $\mathcal{S}_z$ domain into regions in which the floats are light and those in which they are heavy, as indicated by the thin gray lines in Fig. 2.

d. Heat fluxes

1) ADVECTIVE (COVARIANCE) HEAT FLUX

D'Asaro (2003a) derives two methods for computing the surface heat flux from Lagrangian float data. The first is to compute the profile of the advective heat flux:

$$\Phi_A(z) \equiv \rho C_p \langle w\theta \rangle(z) = \rho C_p \langle w\theta' \rangle(z), \tag{6}$$

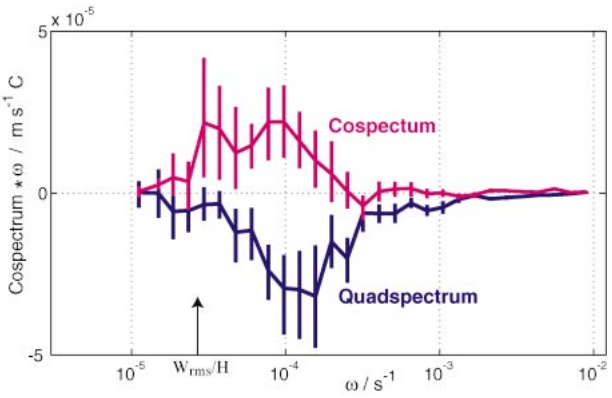

FIG. 3. Cross-spectrum of temperature and vertical velocity for all 1997 and 1998 DLF data plotted in energy-preserving form. The depth-average heat flux is proportional to the area under the cospectrum (red) curve. Confidence limits are 95%.

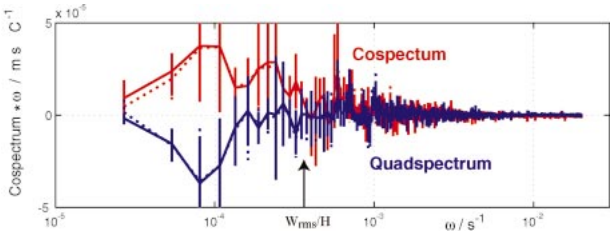

FIG. 4. Average cross-spectrum of temperature and vertical velocity for seven selected MLF 1995 data points plotted in energy-preserving form. Confidence limits are 95%. Two cases are shown: A mean removed from temperature (solid) and a quadratic polynomial removed (dotted).

where ρC_p converts temperature flux to heat, $\theta' = \theta - \overline{\Theta}_{\rm ml}$ is the temperature, and $\overline{\Theta}_{\rm ml}$ is the mixed layer average temperature. For a given segment of float data, $\overline{\Theta}_{\rm ml}$ is computed from a polynomial fit to all temperature data within the mixed layer and then low-pass filtered using a cosine window of length T. The average value of the perturbation temperature θ' and w are then computed exactly in each pass of each float through each depth bin and these values are averaged to form $\Phi_A(z)$. The surface heat flux Q_{0A} is computed by extrapolating $\Phi_A(z)$ to the surface.

The length of the low-pass filter defined by T and the polynomial fit is adjustable. If T is too small, the heat flux carried by lower frequencies will be neglected and the results are biased. If T is too large, the statistical noise becomes larger because the contributions from the lowest frequencies have very few degrees of freedom. Figure 3 shows the cross-spectrum of temperature and vertical velocity for the DLF data plotted in an area-preserving form. A quadratic polynomial has been removed from the temperature. The area under the cospectrum (red) is proportional to the average value of $\Phi_A(z)$. Note that even though the depth variations of the float complicate the interpretation, the cospectrum is still a useful diagnostic of the contribution of various frequencies to the flux. There is little contribution for frequencies less than about 3×10^{-5} s^{-1}, or a period of 2.5 days. Heat fluxes were computed using $T = 8$ days based both on these cospectra and on plots of the heat flux as a function of T. A typical overturning time for these data is $T_0 = H/W_{\rm rms} = 600/0.015 = 0.5$ days, so T is approximately 16 T_0.

Figure 4 shows the cross-spectrum from the 1995 MLF data. There are significant contributions from even the lowest frequency. This is also shown by the significant difference in spectra computed after removing the mean from the perturbation temperature (solid) and after removing a quadratic (dotted) polynomial. The approximately 20-h record lengths may therefore be too short to include all of the covariance. This is surprising because the typical overturning time for these data is $T_0 = H/W_{\rm rms} = 40/0.014 = 0.8$ h, giving a record length of 25 T_0.

Figure 1e shows the profile of $\Phi_A(z)$ (red) for DLF float 8. Through the bulk of the mixed layer, $\Phi_A(z)$ varies linearly with depth, as expected for a uniformly cooling boundary layer. It decreases near the surface as more of the heat flux is carried by unresolved motions. The surface heat flux is computed by fitting a line (shown dashed in Fig. 1e) from 25 m, just below the surface layer to 600 m, approximately the mixed layer base, and extrapolating it to the surface. The resulting surface heat flux Q_{0A} is shown by the red error bar plotted above the surface.

2) DIFFUSIVE HEAT FLUX

A second, less familiar, method is derived by horizontally averaging and integrating the Lagrangian heat equation,

$$\frac{D\theta}{Dt} = \kappa \nabla^2 \theta, \tag{7}$$

noting that the surface heat flux is $Q_0 = \rho C_P \kappa (\partial \langle \theta \rangle / \partial z)$, to obtain

$$\Phi_D(z) \equiv \rho C_p \int_z^0 \left\langle \frac{D\theta}{Dt} \right\rangle dz. \tag{8}$$

The same expression is derived without the assumption of a flat, diffusively controlled surface in D'Asaro (2003b) using a Lagrangian analysis of heat transport. In a classical boundary layer all heat is supplied from the boundary. Thus, $\langle D\theta/Dt \rangle$ is zero except in the surface layer and $\Phi_D(z)$ rises from zero to Q_0 within the surface layer and remains constant in the interior. The surface heat flux Q_{0D} is therefore computed by fitting a line to $\Phi_D(z)$ outside of the surface layer and extrapolating it to the surface, just as is done with $\Phi_A(z)$.

Figure 1e shows the profile of $\Phi_D(z)$ (black) for DLF float 8. As expected, it varies rapidly in a thin near-surface layer. In the interior, however, it is not constant, but decreases steadily, varying by approximately 350

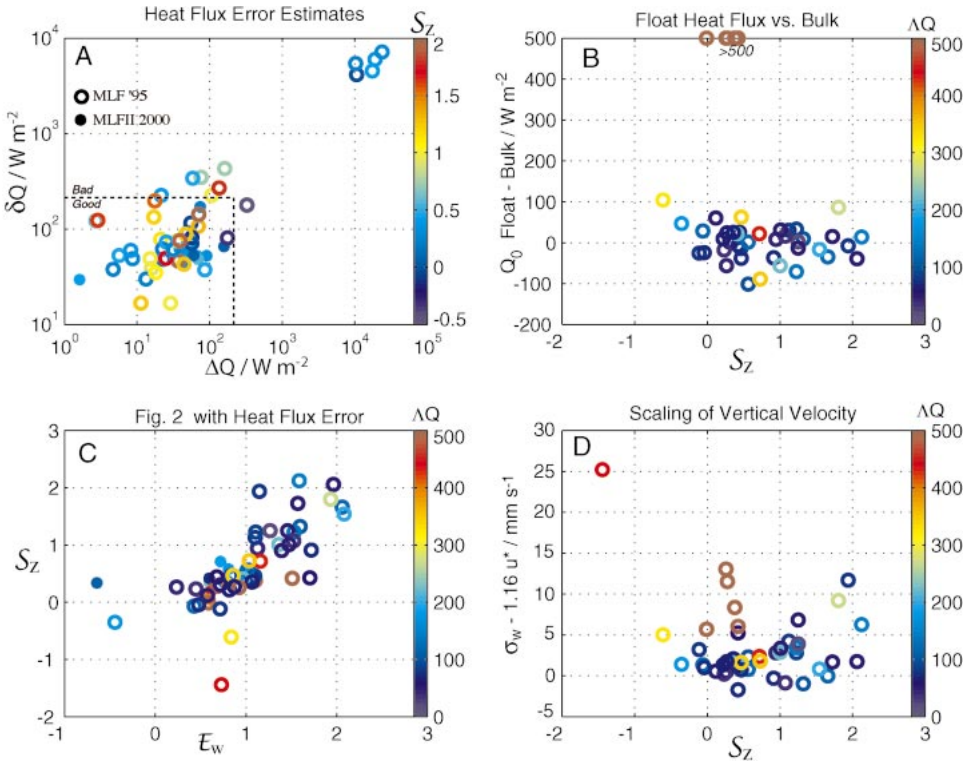

FIG. 5. Error measures. (a) Advective–diffusive difference ΔQ [(11)] vs 70% bootstrap error estimate δQ [(12)]. Color is depth skewness $\mathcal{S}_z$. (b) $\mathcal{S}_z$ vs deviation of float heat flux [(10)] from the bulk estimate. Values greater than 500 W m^{-2} are plotted as 500 W m^{-2}. (c) $\mathcal{S}_z$ vs E_w, as in Fig. 2. (d) Deviation of rms vertical velocity σ_w from $1.16u^*$ (D'Asaro 2001). Color in (b)–(d) is float heat flux error ΛQ [(13)].

W m^{-2} from the near surface to 600 m. This is not always true; D'Asaro (2003b) shows profiles of $\Phi_D(z)$ from two floats deployed on either side of the eye of Hurricane Dennis. One shows no slope in $\Phi_D(z)$, the other has a slope. The presence of a slope implies that the floats are heating or cooling on average at a given depth within the boundary layer interior. If the water is truly heating and because there are no true heat sources in the interior, this apparent heat source must represent the apparent boundary layer heating due to the advection of the float across horizontal temperature gradients. Although this is undoubtedly related to heat fluxes in the boundary layer due to the vertical shear of horizontal currents (Rudnick and Ferrari 1999), a more detailed analysis is beyond the scope of this paper. The extrapolation of a line fit to $\Phi_D(z)$ in the mixed layer interior (shown dashed black in Fig. 1e) is used to compute Q_{0D}, shown by the black error bar plotted above the surface.

3) Error measures

Figure 5 investigates the errors in the heat flux and σ_w measurements. Figures 5a and 5c use both the MLF 1995 data and the MLFII 2000 data, while Figs. 5b and 5d use only the MLF 1995 data. Figure 5a compares the difference between the advective and diffusive heat flux estimates,

$$\Delta Q = |Q_{0A} - Q_{0D}|, \tag{9}$$

and the bootstrap-estimated errors δQ_{0A} and δQ_{0D} combined into

$$\delta Q = (\delta Q_{0A}^2 + \delta Q_{0D}^2)^{1/2}. \tag{10}$$

Each bootstrap error is computed at the 70% level, approximating one standard deviation. They are correlated. Accordingly, a single measure of error,

$$\Lambda Q = \max[\delta Q, \Delta Q], \tag{11}$$

is defined. Note that these errors appear unrelated to the skewness $\mathcal{S}_z$ (colored in Fig. 5a).

Figure 5b plots the deviation of the combined heat flux estimate,

$$Q_{0F} = \frac{1}{2}(Q_{0A} + Q_{0D}), \tag{12}$$

from the surface heat flux computed from the shipboard measurements, Q_{Bulk}. It is unrelated to the skewness $\mathcal{S}_z$, but the outliers are accurately captured by their large values of ΛQ. Similarly, outliers from the relationship between vertical kinetic energy and wind speed (D'Asaro 2001) are captured by ΛQ in Fig. 5d, as are some of the outliers in the scatterplot of $\mathcal{S}_z E_w$ in Fig. 5c. Overall, ΛQ is seen to be an effective tool for rejecting bad data segments, while the skewness $\mathcal{S}_z$ is not.

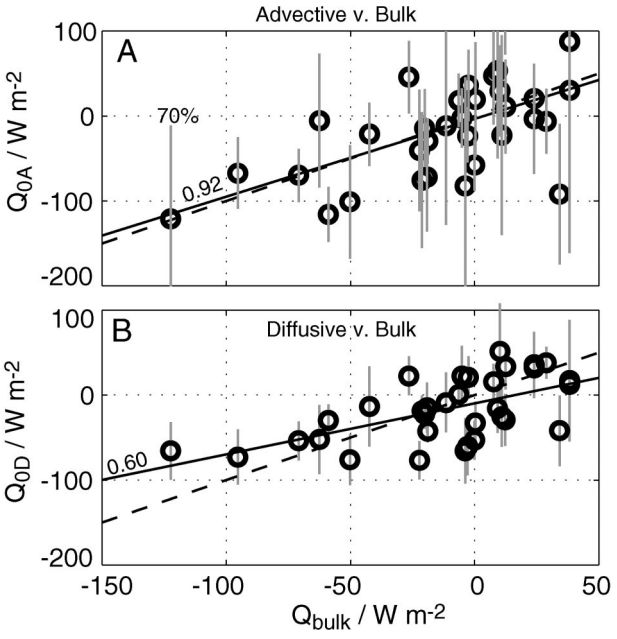

FIG. 6. (a) Comparison of advective Q_{0A} and bulk heat flux for 1995 MLF data. Only data for which $\Lambda Q < 200$ W m^{-2} is plotted. Gray vertical lines are $\pm\ \delta Q_A$, with 70% confidence level bootstrap error estimates. The solid line gives a least squares fit; the dashed line gives a perfect fit. (b) Same as in (a) but for diffusive heat flux Q_{0D}.

4. Comparison of float and bulk heat fluxes

Figure 6 and Table 1 compare Q_{0A} and Q_{0D} with the Q_{Bulk}. On average the float and bulk methods agree to within better than 10 W m^{-2} for both positive and negative heat fluxes, consistent with the statistical uncertainties in the float methods and the probable methodological errors in the bulk method. On a deployment-by-deployment basis (Fig. 6), the float fluxes are clearly correlated with the bulk fluxes, the slope of the best-fit lines being 0.92 for Q_{0A} and 0.60 for Q_{0D}. These slopes are both less than one, consistent with the approximately 20-h-long record lengths being somewhat shorter than necessary to capture all of the flux.

5. Summary and discussion

The ability of Lagrangian floats to measure surface heat flux is investigated using data from winter and fall float deployments in the central Labrador Sea and the northeast Pacific. These floats were only imperfectly Lagrangian so a major emphasis of this study is to develop diagnostics to characterize the ability of the floats to make accurate measurements of averaged turbulent quantities. Major results include the following.

- Floats can measure surface heat flux in two ways: Q_{0A} from the vertical advection of temperature (6) and Q_{0D} from the Lagrangian rate of change of temperature (8).

TABLE 1. Advective and diffusive estimates of Q_0 compared to shipboard bulk estimates. All values in W m^{-2}. Values in parentheses are half-widths of bootstrap confidence intervals at 66% and 95%; N is the number of data points.

Q_{Bulk}		$Q_A - Q_{\text{Bulk}}$	$Q_D - Q_{\text{Bulk}}$	
Range	Mean	Mean (66%/95%)	Mean (66%/95%)	N
All	−22	−4 (9/16)	−5 (6/12)	33
>0	19	6 (14/28)	−12 (11/16)	13
<0	−33	−8 (8/18)	0 (6/16)	20
>20	31	−22 (21/47)	−16 (15/22)	6
<−50	−77	−4 (16/35)	17 (15/20)	6

- Four diagnostics of the ''quality'' of a given set of float measurements were developed: $\mathcal{S}_z$, the skewness of float depth; E_w[(5)], which quantifies whether the vertical kinetic energy computed directly agrees with that computed from the Lagrangian acceleration; ΔQ[(9)], the difference between Q_{0A} and Q_{0D}; and δQ, the statistical error in Q_{0A} and Q_{0D}.
- Both $\mathcal{S}_z$ and E_w are closely related (Fig. 2). Large positive values indicate that the floats are upwardly buoyant. Floats that are neutrally buoyant in the mixed layer have a small positive value.
- Both ΔQ and δQ are closely related (Fig. 5) so that their maximum ΛQ is a useful error measure.
- Large values of ΛQ are a good indicator of poor quality data (Fig. 5).
- When screened by ΛQ the float-measured heat fluxes are well correlated with bulk heat fluxes computed from shipboard data on the one cruise where they are available. On average, both Q_{0A} and Q_{0D} agree with the bulk heat flux to within 10 W m^{-2} and are well within the statistical and bias errors of the measurements.
- Although no systematic errors in the float heat flux measurements with $\mathcal{S}_z$ are apparent, a 20% increase of rms vertical velocity (Fig. 5d) at high $\mathcal{S}_z$ suggests that similar biases in heat flux measurements due to float buoyancy may occur.

This study finds no overwhelming impediments to the measurement of air–sea heat and other scalar fluxes by Lagrangian floats. The techniques outlined here will only work in turbulent oceanic boundary layers that are significantly thicker than the size of the floats. Successful and accurate measurements will require long averaging times particularly given the suggestion in Fig. 4 that record lengths of many days are required for the cospectra to converge. Useful instruments must therefore have a duration of many months at least, as does MLFII, and the ability for the floats to remain accurately neutrally buoyant for extended periods, an ability also demonstrated by MLFII. Proper verification of this technique will require intercomparison, preferably with direct flux techniques, under a variety of conditions for periods of weeks to months.

Acknowledgments. This work was supported by NSF Grant OCE 9711650 and ONR Grants N00014-94-1-0024 and N00014-94-1-0025. The engineering and support staff at the APL–UW has been essential in conducting this work as have the crews of numerous research and commercial vessels.

REFERENCES

D'Asaro, E. A., 2001: Turbulence intensity in the ocean mixed layer. *J. Phys. Oceanogr.,* **31,** 3530–3537.

——, 2003a: Performance of autonomous Lagrangian floats. *J. Atmos. Oceanic Technol.,* **20,** 896–911.

——, 2003b: The ocean boundary layer beneath Hurricane Dennis. *J. Phys. Oceanogr.,* **33,** 561–579.

——, D. M. Farmer, J. T. Osse, and G. T. Dairiki, 1996: A Lagrangian float. *J. Atmos. Oceanic Technol.,* **13,** 1230–1246.

——, K. B. Winters, and R.-C. Lien, 2002: Lagrangian analysis of a convective mixed layer. *J. Geophys. Res.,* **107,** 3040, doi: 10.1029/2000JC000247.

Dickey, T., D. Manov, R. Weller, and D. Siegel, 1994: Determination of longwave heat flux at the air–sea interface using measurements from buoy platforms. *J. Atmos. Oceanic Technol.,* **11,** 1057–1078.

Edson, J., A. Hinton, K. Prada, J. Hare, and C. Fairall, 1998: Direct covariance flux estimates from mobile platforms at sea. *J. Atmos. Oceanic Technol.,* **15,** 547–562.

Efron, B., and G. Gong, 1983: A leisurely look at the bootstrap, the jackknife and cross-validation. *Amer. Stat.,* **37,** 36–48.

Farmer, D. M., and M. Li, 1995: Patterns of bubble clouds organized by Langmuir circulation. *J. Phys. Oceanogr.,* **25,** 1426–1440.

Graber, H., E. Terray, M. Donelan, W. Drennan, J. Van Leer, and D. Peters, 2000: ASIS—A new air–sea interaction spar buoy: Design and performance at sea. *J. Atmos. Oceanic Technol.,* **17,** 708–720.

Harcourt, R. R., E. L. Steffen, R. W. Garwood, and E. A. D'Asaro, 2002: Fully Lagrangian floats in Labrador Sea deep convection: Comparison of numerical and experimental results. *J. Phys. Oceanogr.,* **32,** 493–510.

Lab Sea Group, 1998: The Labrador Sea deep convection experiment. *Bull. Amer. Meteor. Soc.,* **79,** 2033–2058.

Lherminier, P., R. Harcourt, R. W. Garwood, and J.-C. Gascard, 2001: Interpretation of mean vertical velocity measured by isobaric floats during deep convective events. *J. Mar. Syst.,* **29,** 221–237.

Lien, R. C., E. A. D'Asaro, and G. T. Dairiki, 1998: Lagrangian frequency spectra of vertical velocity and vorticity in high-Reynolds number oceanic turbulence. *J. Fluid Mech.,* **362,** 177–198.

Renfrew, I., G. Moore, P. Guest, and K. Bumke, 2002: A comparision of surface layer and surface turbulent flux observations over the Labrador Sea with ECMWF analysis and NCEP reanalyses. *J. Phys. Oceanogr.,* **32,** 383–400.

Rudnick, D., and R. Ferrari, 1999: Compensation of horizontal temperature and salinity gradients in the ocean mixed layer. *Science,* **283,** 526–529.

Steffen, E., and E. D'Asaro, 2002: Deep convection in the Labrador Sea as observed by Lagrangian floats. *J. Phys. Oceanogr.,* **32,** 475–492.

Stommel, H., 1949: Trajectories of small bodies sinking slowly through convection cells. *J. Mar. Res.,* **8,** 24–29.